Proposal to DESY

for a

Longitudinal Electron Polarimeter

at

HERA — East Section

by the

HERMES collaboration

(May 1995)

W. Lorenzon

ABSTRACT

We propose to build a longitudinal polarimeter for the HERMES experiment at the DESY laboratory in Hamburg, Germany. The longitudinal polarization will be measured directly using multi-Compton photon backscattering of circularly polarized pulsed laser light off the electron beam, then measuring the energy weighted asymmetry in the backscattered photons. The proposed equipment will be built by the medium energy nuclear physics group at the University of Pennsylvania in collaboration with the University of Freiburg. We have performed detailed studies and present a technical solution to implement such a device in the present electron storage ring. It is expected to yield higher accuracy than the transverse polarimeter and will provide an independent measurement of the electron beam polarization.

Contents

I. INTRODUCTION

The HERMES proposal to employ polarized gas targets in the HERA electron storage ring at DESY originated in groups at Caltech and the Max Planck Institute in Heidelberg in 1988. This proposal involves the use of newly developed polarized gas target technology to perform measurements of spin-dependent deep inelastic scattering with high statistical and systematic precision. A full proposal was submitted to DESY in 1990, and after demonstration of both polarized beam in the ring and polarized target feasibility, full approval was granted in September of 1992. The physics motivation, experimental design and other issues are detailed in the HERMES Technical Design Report to DESY [1].

The HERMES collaboration is competing internationally with the SMC collaboration at CERN and with the E142/43 and E154/55 collaborations at SLAC to measure the spin structure functions of the nucleons and to test the Bjorken sum rule. The HERMES experiment, which is using the newly developed gas target technology, has some advantages for measuring the spin structure functions of the nucleons, among which are:

- no dilution by unpolarized target material,
- small radiative corrections,
- rapid target spin reversal,
- measurement of beam polarization with systematic errors smaller than 3%.

It is interesting to compare the systematic errors we hope to achieve with HERMES to the systematic uncertainties of the competing experiments, see Table 1.

Table 1. Sources of systematic errors to $\int g_1^p(x)dx$ together with the statistical errors are shown as reported by SMC and E143. These errors are compared with the anticipated statistical and systematic errors for HERMES and E155 (taken from their proposal).

Experiment	statistics	dilution	rad. corr.	P_T	P_B	total systematics
SMC	8.1%	2.5%	1.7%	2.9%	4.2%	8.1%
E143	3.0%	$< 3\%$	2%	2.7%	3.6%	9.0%
HERMES	2.3%	–	1.2%	3.0%	2.5%	5.2%
E155	1.1 %	2%	2%	2%	3%	6%

The dominant sources for systematic uncertainties in all four experiments are the beam and target polarizations. The systematic uncertainties for the beam polarization measurements reported by the HERA polarimeter group are 8% [2]. The beam polarization measurement is performed by measuring small spatial asymmetries in Compton backscattered photon distributions. This is a measurement of the degree of transverse polarization of the electron beam. A task force has been formed to study the sources of the large systematic uncertainties and subsequently attempt to reduce this number to below 3%.

It is crucial for HERMES to measure the beam polarization with as small a systematic error as possible. The best way to achieve this is to do two independent measurements of the beam polarization. We therefore propose to measure the longitudinal polarization in the HERA East Section, independent of the transverse polarization measurement by also using Compton backscattering of circularly polarized laser light off the electron beam, and then measuring the energy asymmetries in the scattered photon distributions. In contrast to the small spatial asymmetries encountered in the transverse polarization measurement, the energy asymmetries are large, up to 0.6 (see Fig. 4). This will allow us to perform measurements with expected systematic uncertainties of about 2-3%. A 1% measurement has been demonstrated at SLAC [3].

Due to large bremsstrahlung backgrounds, resulting from interactions of the electron beam with the HERMES gas targets and vacuum rest gas, the multi-photon method will be adapted. For the transverse polarimeter, the single photon method is used because the backgrounds are considerably smaller.

II. THE LONGITUDINAL ELECTRON POLARIMETER

A. Polarization at HERA

In electron storage rings the electron spin can become polarized antiparallel to the magnetic bending field as a result of synchrotron radiation emission (Sokolov-Ternov effect [4]). The polarization increases in time according to

$$P(t) = P_{\max}(1 - e^{-t/\tau}), \tag{1}$$

where τ is the polarization build-up time and $P_{\max}$ is the equilibrium polarization. In an ideal flat machine and in the absence of depolarizing effects the maximum polarization achievable is 0.924. In the presence of the HERMES spin rotators, however, the maximum polarization is reduced to 0.894 [5].

In a real machine, there are also strong depolarizing effects which can counteract the Sokolov-Ternov effect. The main source of the depolarization is again the emission of synchrotron radiation which excites incoherent oscillations in the particle orbits. In a real machine with closed orbit distortions, the magnetic field on the closed orbit is not exactly vertical and the spin axis can be tilted by tens of milliradians. In the presence of stochastic orbit motion this causes diffusion of the spins [6], which can lead to depolarization. The strength of this depolarizing process can be quantified with a time constant of the diffusion, τ_D. This process works simultaneously with the Sokolov-Ternov build-up, and the value of the asymptotic polarization $P_{\max}$ is determined by the relative strengths of the two processes according to

$$P_{\max} = P_{\rm ST}\frac{\frac{1}{\tau_{\rm ST}}}{\frac{1}{\tau_{\rm ST}} + \frac{1}{\tau_{\rm D}}}. \tag{2}$$

The effective build-up time τ is also reduced by spin diffusion to

$$\frac{1}{\tau} = \frac{1}{\tau_{\rm ST}} + \frac{1}{\tau_{\rm D}}. \tag{3}$$

The best way to measure the electron beam polarization is to backscatter circularly polarized laser light off the electron beam and to measure the asymmetry in the scattered photon distributions.

The transverse polarization of the HERA electron beam has been measured in the West Hall, and a polarization of $P_y = 0.56 \pm 0.016(\text{stat.}) \pm 0.05(\text{syst.})$ has been reported [7] initially. At present the systematic uncertainties of the beam polarization are quoted to be 8% [2], which would be the largest contribution to the systematic uncertainties expected by HERMES in the extraction of the polarized structure functions. Typical other systematic uncertainties are expected in the order of $1\% - 3\%$, leading to a total expected systematic uncertainty of 4.3% in the Bjorken sum rule [1]. It is believed, however, that the systematic uncertainty in the transverse polarization measurement can be reduced to below 3% by the following feature of the Sokolov-Ternov effect, assuming stable beam, calorimeter and laser conditions.

By rearranging Eq. 2 and 3,

$$P_{\max} = \tau\left(\frac{P_{\rm ST}}{\tau_{\rm ST}}\right), \tag{4}$$

it follows that the measurement of the build-up time can provide a separate measurement of the polarization. Assuming that the Sokolov-Ternov calculation of the build-up time is exact, even for a non-flat machine, the spatial asymmetries can be calibrated using the characteristic rise-time behaviour.

However, Eq. 2 is not exact. There is an extra factor $(1+\delta)$ in the numerator. This can be seen by inspecting the Derbenev-Kondratenko formula [8] which generalizes the Sokolov-Ternov formula to take depolarizing effects into account. When the spin rotators are off, δ is so small that it can be neglected. With the spin rotators on, δ can be several percent. δ cannot be estimated reliably; it is a function of the sources of depolarization, which are not well known. The factor $(1+\delta)$ feeds through into Eq. 4 and therefore, Eq. 4 cannot provide a reliable way to calibrate a polarimeter at the percent level when the spin rotators are on. This means that the calibration of the transverse polarimeter must be done with the spin rotators switched off (this is not the standard operating mode of HERMES!). Incidentally, with the calibrated transverse polarimeter and the new longitudinal polarimeter we can measure this quantum mechanical correction which is so difficult to calculate [5].

In May 1994 the spin rotators in HERA East were turned on, and 0.5 polarization was measured without any further machine adjustments. Since then electron beam polarizations up to 0.7 have been measured. This is substantially higher than previously predicted.

In October and November 1994, 14 rise-time measurements were performed with dedicated beam where polarizations between 0.3 – 0.6 with 1% – 2% statistical errors were recorded. For ideal conditions, Eq. 1 can be written as

$$k \cdot P(t) = P_{\max}(1 - e^{-t/\tau}), \tag{5}$$

with the calibration constant k=1. For each rise-time measurement the calibration constant k was extracted [2,9]. Ideally, one expects $< k >$=1 and the distribution of k to be statistical. The HERA polarimeter group reported a value for $< k >$ of 1.03 (so the polarization has been overestimated by 3%) but more surprisingly, the root mean square distribution came out to be 8%. This is far bigger than what one expects from statistical distributions.

B. Compton Scattering

Compton-laser polarimeters utilize the spin-dependent cross section for Compton scattering of polarized photons on electrons. The differential Compton cross section can be written as a function of the initial electron and photon polarizations **P** and **S**. The kinematics are shown in Fig. 1. Due to the large relative horizontal smearing of the backscattered photon distributions, the horizontal distribution is not measured and thus summing over x leads to [10]

$$\frac{d\sigma_c}{d\Omega}(\mathbf{S},\mathbf{P}) = \frac{1}{2} r_0^2 \left(\frac{k_f}{k_i}\right)^2 \left[\Sigma_0 + S_1(0)\Sigma_1 + S_3(P_{\rm Y}\Sigma_{2\rm Y} + P_{\rm Z}\Sigma_{2\rm Z})\right], \tag{6}$$

where

$$\Sigma_0 = (1 + \cos^2\theta) + (k_i - k_f)(1 - \cos\theta),$$

$$\Sigma_1 = \cos 2\phi \sin^2\theta,$$

$$\Sigma_{2\rm Y} = -k_f \sin\phi \sin\theta (1 - \cos\theta),$$

$$\Sigma_{2\rm Z} = (1 - \cos\theta)(k_f + k_i)\cos\theta,$$

with S_1 and S_3 the linear and circular components of the initial photon polarization and $P_{\rm Y}$ and $P_{\rm Z}$ the vertical and longitudinal components of the initial electron polarizations. r_0 is the classical electron radius and k_i, k_f are the initial and final photon momentum in the rest frame. Σ_0 is the unpolarized cross section, Σ_1 and $\Sigma_{2\rm Y}$ depend on the azimuthal scattering angle ϕ and are used for the vertical polarization measurement, and $\Sigma_{2\rm Z}$ is used for the longitudinal polarization measurement.

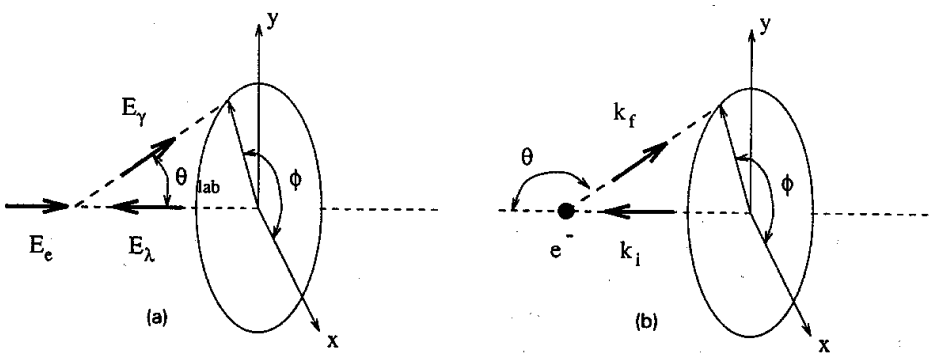

Figure 1. Geometry and coordinate system of Compton scattering, showing the lab (a) and rest frame (b) scattering angles of the photon. The final electron is not shown.

C. Measurement of Transverse Polarization

The calorimeter for the transverse polarimeter has been designed specifically to measure very small spatial asymmetries [11]. The calorimeter is split into two parts, an upper and a lower part. The energy of the incoming photon is the sum of the energies of the two halves, $E_\gamma = E_u + E_d$, and the vertical position is measured using the asymmetry of the energies

$$\eta(y) = \frac{E_u - E_d}{E_u + E_d}, \tag{7}$$

and the η-to-y transformation of Fig. 2. The vertical component of the electron polarization ($P_{\rm Y}$) is measured using the asymmetry of the Compton cross section for scattering of vertically polarized electrons off circularly polarized photons. There are two ways of measuring the vertical polarization:

1. The vertical polarization can be obtained from measurements of the spatial asymmetry

$$\mathcal{A}(y, E_\gamma) = \Delta S_1 \Sigma_{1/0} + \Delta S_3 P_{\rm Y} \Sigma_{2{\rm Y}/0}, \tag{8}$$

   with $\Delta S_1 = \frac{1}{2}(S_{1,L} - S_{1,R})$, where $S_{1,L}$ and $S_{1,R}$ are the degrees of linear polarization of the laser light. Note that the spatial asymmetry measurement not only depends on the circular, but also the linear component of the laser light.

2. The polarization $P_{\rm Y}$ can also be obtained from the shift of the mean vertical positions $\langle y \rangle$ measured with left and right circularly polarized light

$$\Delta y(E_\gamma) = \frac{1}{2}(\langle y \rangle_{\rm L} - \langle y \rangle_{\rm R}) = P_{\rm Y} \Delta S_3 \Pi(E_\gamma). \tag{9}$$

   The analyzing power $\Pi(E_\gamma) \leq 200 \mu m$, which is equal to the shift measured when $\Delta S_3 P_{\rm Y} = 1$, has been derived using the η-to-y transformation. This is the method usually used to report measurements of $P_{\rm Y}$. The η-to-y transformation used in the present online analysis was obtained experimentally in 1990, when the detector was put into a 1–3 GeV test beam [10].

The statistical error in the transverse polarization $\delta P_{\rm Y}$ is given by [10]

$$\delta P_{\rm Y} = \frac{1}{\Delta S_3 \Pi} \frac{\sigma_Y}{\sqrt{N}}. \tag{10}$$

The transformation function $\eta(y)$ is not a linear function of the $y-$position of the incoming photons(see Fig. 2) and depends somewhat on the properties of the electron beam. The uncertainty in this transformation function is one of the largest sources of systematic errors of the vertical polarization measurement [7,10]. Detailed Monte Carlo simulations are being performed to better understand the transverse polarimeter. This should help to assess a realistic error to the transverse polarization measurements.

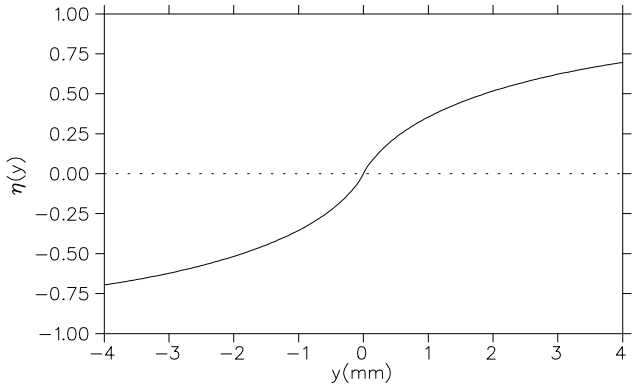

Figure 2. The transformation function $\eta(y)$.

D. Measurement of Longitudinal Polarization

In contrast to the small spatial asymmetry measured with the transverse calorimeter, the measurement of the longitudinal polarization ($P_{\rm Z}$) is based on large asymmetries in the energy distributions of the scattered photons. The energy spectra with longitudinal electron polarization $P_{\rm Z} = 1$ and photon polarization $S_3 = \pm 1$ are shown in Fig. 3.

The integrals of Σ_1 and $\Sigma_{2\rm Y}$ over y are zero so the general form of the asymmetry of energy spectra can be written as

$$\mathcal{A}(E_\gamma) = \Delta S_3 P_{\rm Z} \Sigma_{2{\rm Z}/0}. \tag{11}$$

The energy asymmetry function $\Sigma_{2{\rm Z}/0}$ is shown in Fig. 4. It is symmetric around z and so no spatial asymmetry has to be measured. The longitudinal polarization $P_{\rm Z}$ can be obtained from the asymmetry in the integrated energies under reversal of the laser photon helicities. For this only a shower counter is needed.

We propose using a pulsed YAG laser (Coherent - Infinity). The primary wavelength of this laser is 532 nm. The maximum backscattered photon energy is 13.6 GeV for a 27.5 GeV electron beam. The total Compton scattering cross section σ_c is 377 mb. The detectable backscattered photons are contained in a narrow cone centered along the direction of the initial electron momentum with angles between 0° (corresponding to $\theta = 180^\circ_{\rm cm}$ and 13.6 GeV) and the critical angle $\gamma^{-1} = 19\mu$rad ($\theta = 90^\circ_{\rm cm}$, 9.1 GeV).

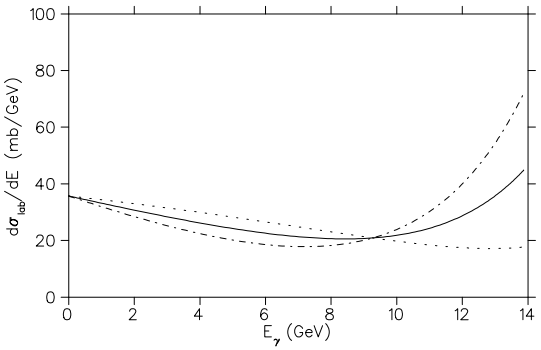

Figure 3. Energy spectra of the scattered photon in the lab frame for Compton scattering. The solid curve is the spectrum for scattering with unpolarized electrons. Overlaid are the spectra for scattering with longitudinally polarized electrons for the cases of $S_3 P_{\rm Z} = +1$ (dotted curve) and $S_3 P_{\rm Z} = -1$ (dash-dotted curve).

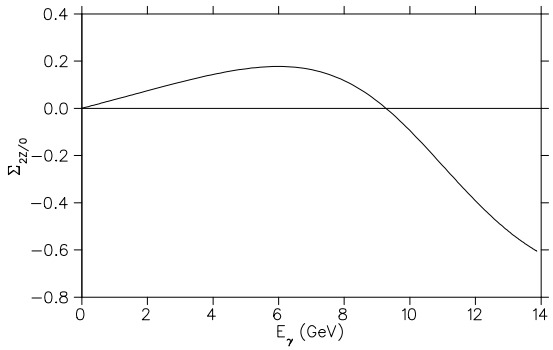

Figure 4. The energy asymmetry function $\Sigma_{2{\rm Z}/0}$ plotted versus the photon energy E_γ. The zero crossing occurs at $90^\circ_{\rm cm}$ and the end point energy corresponds to $180^\circ_{\rm cm}$.

The YAG model from Coherent has two features which have only become available during the last year. Due to thermal lensing effects inside the YAG rod, it has not been possible so far to change either the laser repetition rate or the pulse energy. The Infinity model incorporates a completely new technology which makes it possible to change the repetition rate between 1–100 Hz and the pulse energy from 0–250 mJ. Due to the large bremsstrahlung background, see Section H.2, the multi-photon method is used. In contrast to the single photon method, where the energy of every individual Compton photon is analyzed, the multi-photon method measures the total energy deposited in the detector by $10^3 - 10^4$ Compton photons per bunch. Therefore, we measure an energy weighted asymmetry

$$\mathcal{A}(\Sigma E_\gamma) = \Delta S_3 P_{\rm Z} \Sigma_{\rm Z_{l_r}}, \tag{12}$$

with

$$\Sigma_{\rm Z_{l_r}} = \frac{\Sigma_l - \Sigma_r}{\Sigma_l + \Sigma_r}, \quad \text{and} \quad \Sigma_i = \int_{E_{min}}^{E_{max}} \left(\frac{{\rm d}\sigma}{{\rm dE}}\right)_i \cdot {\rm E} \cdot {\rm dE}, \quad \text{where} \quad i = l, r.$$

The energy weighted asymmetry $\mathcal{A}(\Sigma E_\gamma)$ is 0.184 for $S_3 P_Z = 1$. The energy weighted spectra with longitudinal electron polarization $P_{\rm Z} = 1$ and photon polarization $S_3 = \pm 1$ are shown in Fig. 5. The average

energy deposited per Compton photon is 6.8 GeV. Assuming 1000 backscattered Compton photons, 6820 GeV is deposited in the calorimeter for an unpolarized electron beam. For the two helicity states, one measures two peaks separated by 1770 GeV for a 0.70 polarized electron beam, as shown in Fig. 6. (Recall, for the transverse polarimeter, a spatial shift of 100μ has to be detected). The measured energy peak positions depend on the luminosity, and the electron and laser polarizations, P_Z and S_3. The asymmetry is determined from the centroids of these two peaks. Note that it is not necessary to know the absolute energy scale, it is sufficient to know that the energy scale is linear. Note also that the absolute position of the two peaks scales with luminosity.

The statistical error in the longitudinal polarization $\delta P_{\rm Z}$ is given by

$$\delta P_{\rm Z} = \frac{1}{\Delta S_3 \langle \Sigma_{\rm Z_{1r}} \rangle} \frac{1}{\sqrt{N}}. \tag{13}$$

To achieve a statistical accuracy $\delta P_{\rm Z}$ of 0.01, assuming $\langle \Sigma_{\rm Z_{1r}} \rangle = 0.1$, requires $N = 10^6$. Assuming a repetition rate of 100 Hz and 5000 backscattered Compton photons per bunch, a measurement takes about 2 s (assuming no background). That is almost an order of magnitude faster than with the transverse polarimeter. This could be an important factor in reducing systematic errors, because it allows us to do many redundant measurements.

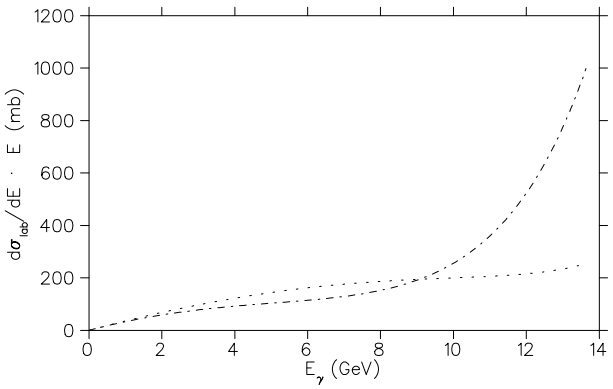

Figure 5. Energy weighted spectra of the scattered photons in the lab frame for scattering with longitudinally polarized electrons for the cases of $S_3 P_{\rm Z} = +1$ (dotted curve) and $S_3 P_{\rm Z} = -1$ (dash-dotted curve).

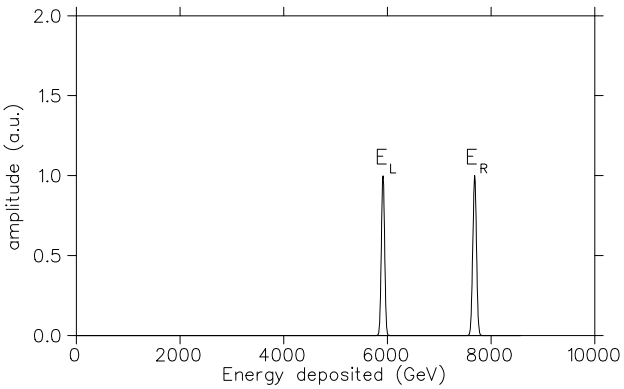

Figure 6. Integrated energy spectra for 1000 scattered Compton photons for the cases of $S_3 P_{\rm Z} = +0.70$ (left peak) and $S_3 P_{\rm Z} = -0.70$ (right peak). The two peaks are separated by 1770 GeV. The resolution of the peaks is expected to be about 3%. The bremsstrahlung peak cannot be seen on this plot, as it is expected to be at 26 ± 11 GeV.

E. Systematic Uncertainties

The main goals of building a longitudinal polarimeter are simplicity of use, ease of analysis, and a low systematic error in the determination of the longitudinal electron polarization.

The sources of systematic errors for the transverse and longitudinal polarimeters are quite different, due to their different requirements: the transverse polarimeter has to measure small spatial asymmetries whereas the longitudinal polarimeter has to measure energy asymmetries.

One should note that the uncertainty in the knowledge of the laser polarization at the interaction point (IP) is common to all types of electron beam polarization measurements, whether we use transverse or longitudinal, single or multi-photon methods. This is also the largest systematic error reported by the SLD group [3] (0.6%). We assume that we can make a 1% measurement.

The largest contributions to the uncertainties in the transverse polarization measurements come from the $\eta(y)$ transformation and from position smearing effects due the electron spot size projected to the position of the calorimeter [7,10]. Neither of these sources has a systematic effect on the longitudinal polarization measurements, since no spatial asymmetry has to be detected.

The multi-photon longitudinal polarimeter has a different set of systematic uncertainties. It measures energy differences and is sensitive to helicity dependent luminosity changes. There are two main classifications of systematic errors: those that cause instrumental asymmetries and those that lead to polarization scale errors.

1. Instrumental asymmetries:

   - A very important consideration in the multi-photon method is the position and intensity stability of the laser beam when switching the polarization with the Pockels cell.

     If the Pockels cell is poorly aligned a change in the voltage across the cell can shift the position of the laser beam horizontally at the IP. This would result in a helicity dependent luminosity if the shift is not very small compared to the widths of the electron and laser beams. This problem has been solved for the transverse polarimeter and shifts of about 8μm have been measured. The shift in the laser beam can be measured with position sensitive detectors.

     The optics system might have a different transparency for different polarization states which would introduce false energy asymmetries. The effect may come from the mirrors which always have different reflectivity for s/p polarization states. This is an important issue in any rate-dependent polarization measurement and solutions to that problem have been found [12]. A feedback system is used to fine tune the phase parameter in a Pockels cell and systematic errors due to that effect could be reduced to $< 0.1\%$.

   - The beam pointing stability of an Argon-Ion laser is about five times better than for a YAG laser. However, the total laser path length for the longitudinal polarimeter is 72 m as compared to about 200 m for the transverse polarimeter. No problems have been reported by the transverse polarimeter group with beam pointing stabilities, and SLD has quoted [3] a 0.5% systematic uncertainty for beam pointing stability with their YAG laser (their laser path length is 41 m). We could therefore assume a systematic uncertainty of about 1%. The Coherent laser company claims, however, that their YAG model has a better beam pointing stability than any competitor's YAG laser, and using an expanded laser beam also helps to improve beam pointing stability. SLD does not use an expanded beam, whereas we have planned to use a 2:1 or 3:1 expansion of the laser beam. So we believe that the systematic uncertainty in the beam pointing stability is around 0.5%.

   - One also has to consider vertical drifts of the laser or electron beam at the IP. This can influence the measured rate due to changes in the beam profiles (Fig. 10), which lead to changes in the luminosity. A drift of 1 mm in the laser beam shifts the IP by about 18 cm. This can lead to a 1.5% change in rate. However, as long as the time constants for these drifts are long compared to the laser helicity switching time (1–100 Hz), the systematic errors induced are very small ($< 0.5\%$).

     The effects discussed above can also be determined by measuring the instrumental asymmetry with an unpolarized electron beam. The electron beam can be depolarized to less than 1% using depolarization bumps. It is also possible to use linear polarized laser light, while still switching the Pockels cell, by removing the $\lambda/4$ after M5 (see Fig. 8). This also will allow us to measure the instrumental asymmetry. Remember from Eq. 11, that either S_3 or P_Z can be set to zero to measure the instrumental asymmetry. Both tests will be done.

2. Polarization scale errors:

   - The rate in the calorimeter can change by up to a factor of ten, due to changes in electron and laser beam intensities. This can put stringent requirements on the linearity and gain stability of the PMT's. The exponential loss of the beam current can partially be compensated for by increasing the laser power in order to keep the luminosity constant. The linearity and gain stability can be measured and the error in that measurement is expected to be smaller than 1% (SLD reports 0.5% for electron detection).

     The linearity of the calorimeter will be measured by sweeping the laser intensity over a wide range and comparing the laser intensity with the detector response. The laser intensity can easily be measured to a fraction of a percent.

   - Pulsed YAG lasers may have large pulse-to-pulse intensity variations which makes it very important to normalize left/right intensities. This is typically done by separating off a small fraction of

the laser beam. The laser intensity can be measured very accurately. So a systematic uncertainty of about 0.1% is assumed (SLD also reports 0.1%, even with no injection seeding). In order to reduce pulse-to-pulse intensity variations, pulsed YAG lasers can be equipped with an injection seeder. Coherent again claims that their new technology renders the smallest pulse-to-pulse intensity variations in the industry.

- The electron beam current can change up to 20% between different bunches. In order to study rate dependent effects we need to know how many bunches are contained in the beam and also their relative intensities. There are many beam position monitors installed along the HERA ring (containing four pick-up electrodes). These monitors also can provide a very accurate timing signal ($\sim$ 50 ps) which is needed to synchronize the laser pulses with the electron bunches. Special pick-up electrodes allow a measurement of the relative intensities to better than 1% [13]. Since we can switch the Pockels cell randomly and we have to choose the bunch the laser will interact with, the correction to that effect is then expected to be about 0.1% [3]. We can also measure the polarization of every single bunch and thus determine if different bunches have slightly different polarizations.
- Another systematic error can arise from variations in the beam optics parameters (α and β). A change in the α and β functions changes the Compton photon distribution on the face of the calorimeter. If the calorimeter cannot absorb all the energy of the Compton photons (due to small size), the energy weighted asymmetry can change by up to 2% for a 10% change in α and β. This is however to be considered an upper limit. The systematic error could be reduced by using a larger detector. But space limitations at the proposed calorimeter position (106 m from the HERMES target) don't allow the use of larger detectors.

It has been shown that a number of redundant tests can be performed to get tight constraints on systematic uncertainties. From the effects discussed above we estimate that we can do a measurement with systematic uncertainties of about 2.5%, see Table 2.

Table 2. List of expected systematic errors to the longitudinal polarization P_Z. Also shown are errors reported by SLD (SLAC Large Detector) [3].

Contribution	SLAC (SLD)	HERA
laser polarization	0.6%	1%
laser beam pointing stability	0.5%	0.5%
laser intensity fluctuations	0.1%	0.1%
laser steering effects (optics system)	0.1%	0.1%
electron orbit stability	n/a	0.5%
PMT linearity and stability	0.5%	1%
electron beam current	0.1%	0.1%
electron beam optics stability	0.1%	<2%
Total	1.0% reported	2.5% estimated

F. The Longitudinal Polarimeter

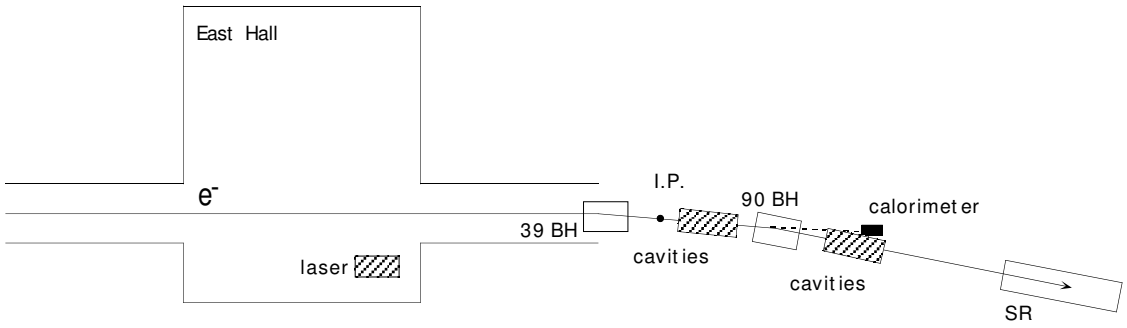

Figure 7. An overview of the longitudinal polarimeter in the HERA East Hall.

A schematic overview of the polarimeter is shown in Fig. 7. It is proposed to situate the laser in a hut about 2 m above the East Hall floor, 8 m from the south wall of the hall. The electron-photon interaction point (IP) is 52 m downstream of the HERMES target, between the first bending magnet 39 BH (0.5 mr) and the beginning of the cavities. 39 BH rotates the spin by 1.8° from the longitudinal direction at 27.5 GeV (spin tune is 62.5). This reduces the measured longitudinal spin component by less than 0.1% ($\cos 1.8°$). The backscattered photons leave the IP traveling in the same direction as the electron beam through the first set of cavities. The two beams are then separated in the second bending magnet 90 BH (2.7 mr). At the end of cavity 105 CA, see Table 3, the beams are separated enough for the photons to exit the vacuum chamber through a 2 mm thick copper window. The detector will be located 54 m from the IP between 105 CA and 107 QL (which will be replaced with a shorter quadrupole (76 cm long) to gain some additional space for the calorimeter), and will be protected with lead and tungsten shielding, see Fig. 13. At that point the two beams are separated by about 4.2 cm.

1. The Optical System

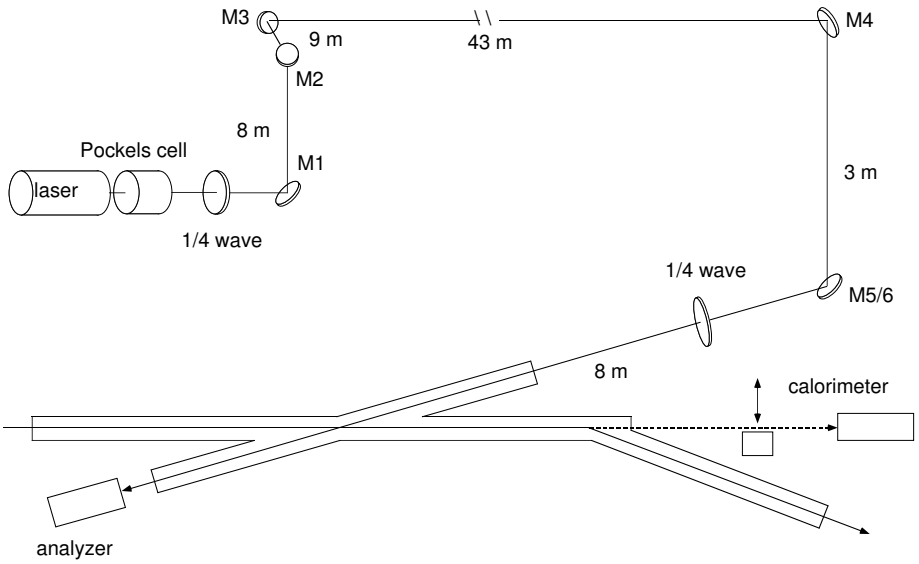

Figure 8. Schematic overview of the optical transport and detector systems.

The optical system will be built following very closely the modified optical system of the transverse polarimeter [14]. A schematic overview is shown in Fig. 8. We propose using a pulsed YAG (Infinity, 40 W, Coherent Corporation) laser. For the electron polarization measurements the frequency doubled light at 532 nm (2.33 eV, green) is used. The laser is located in a hut in the East Hall and the laser beam is steered

to the IP by means of six dielectric mirrors. The laser is mounted in the laser hut parallel to the electron beam, 2 m above ground [15]. This allows us to use the mirrors M1/M2, M3/M4 and M5/M6 as pairs with perpendicular reflection planes. This is an elegant trick to compensate phase shifts in the reflection of dielectric mirrors to a large extent. The first mirror M1 deflects the beam up by 90° to the tunnel ceiling height. At M2 the beam gets deflected by 90° towards the tunnel and another deflection of 90° at M3 directs the beam 43 m through the tunnel along the ceiling to M4. There, the beam is deflected from the tunnel ceiling down to the electron ring and M5/M6, which are only a few centimeters apart to form a phase-compensated pair, direct the beam through the entrance window into the electron vacuum chamber. After passing through the IP the beam exits the vacuum system through a second vacuum window and enters a polarization analyzer, which also monitors the position and intensity of the laser light.

2. Compton Detector System

The Compton detector should be able to detect photons from 1 GeV up to 30 GeV with good energy resolution, handle rates of 10 MHz and be radiation resistant. It should also be able to detect multiple photon signals with integrated energies of 10 TeV. We propose to use the same type of calorimeter which is used for the HERMES luminosity monitor system (for details see HERMES Technical Design Report). The response of those $NaBi(WO_4)$ (also called NBW) crystals has been measured at DESY and has been simulated using the GEANT Monte Carlo code. We find that the resolution for 1–15 GeV photons is independent of length for 15–20 cm long crystals. Ideally we would like to use a 20 cm long (19 X_0), 7 cm diameter single crystal, however, the manufacturer in Moscow can only produce 3.2 cm wide cylindrical crystals. Due to space limitations we decided to get four 2.2×2.2 cm^2 crystals arranged in a 2×2 array (Fig. 13). This will allow precise alignment of the NBW array on the backscattered photon beam. The radiation hardness of the material is very high (7×10^7 rad), the energy resolution (σ) about $10\%/\sqrt{E(\mathrm{GeV})}$ [16] and the Moliere radius 2.38 cm. It will be energy calibrated using the DESY test beam at different electron energies and possibly using beam-target bremsstrahlung. The HERMES gain monitoring system will be used to check for gain shifts between calibrations. This system is also important for continuous monitoring of the helicity dependence of the gain due to rate effects.

G. Installation of Polarimeter in HERA – East

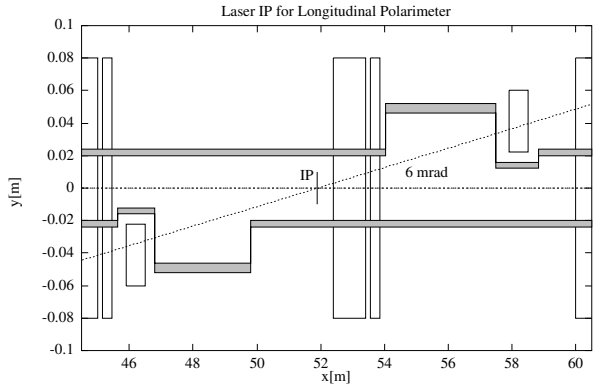

Figure 9. Sideview of the beam line in the electron-photon interaction region. Modifications to the beam line for the IP at 51.9 m from the target are shown. Note, quadrupoles and corrections coils are not to scale.

The choice of a suitable electron-laser interaction region is determined by the fact that the backscattered rate should be maximized and stable. Maximizing the Compton rate means that the crossing angle α between the laser beam and the electron beam, and the horizontal widths of the electron and laser beams should be as small as possible in order to maximize the luminosity of the interaction [10]. At the same time the measured Compton rate should be insensitive to small shifts in the laser and electron beams. In addition, the electrons in the interaction point (IP) are not all located at $x = y = 0$ traveling parallel to the z axis. The effective smearing of the backscattered distributions due to the distributions in position and direction

of the initial electrons has to be minimized, since the backscattered photons have to get through a number of quadrupole magnets and cavities before they exit the vacuum system. We also would like to minimize changes to the electron ring vacuum system.

Considering these constraints, we propose the following scenario for the IP. The IP is located just upstream of 53 QL at 51.9 m (Fig. 9) with a crossing angle $\alpha = 6$ mr. The laser light enters the vacuum system from the top at about 58 m from the target and exits through the bottom at about 47 m from the target. The modification to the beam line is shown in Fig. 9 [17].

Fig. 10 shows the horizontal and vertical electron beam widths in HERA East between 45 QL and 61 QL. The horizontal and vertical widths of the backscattered photons from the IP are displayed in Fig. 11. The beam optics parameters at the IP are $\alpha_x = 0.596$, $\beta_x = 8.15$ m, and $\alpha_y = -1.533$, $\beta_y = 25.24$ m.

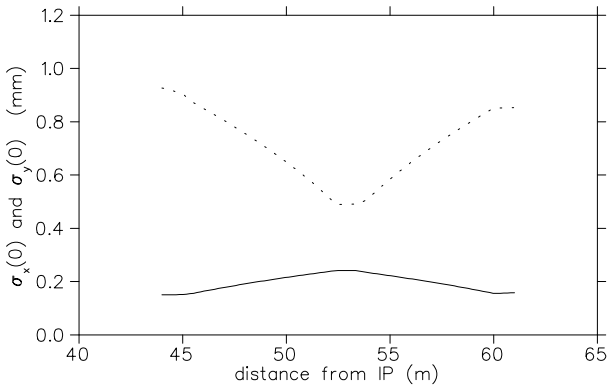

Figure 10. The horizontal (dotted line) and vertical (solid line) electron beam widths in the electron-photon interaction region. The minimum in $\sigma_x(0)$ occurs inside quadrupole 53 QL. The ratio of vertical to horizontal emmitance is assumed to be 0.065 [18].

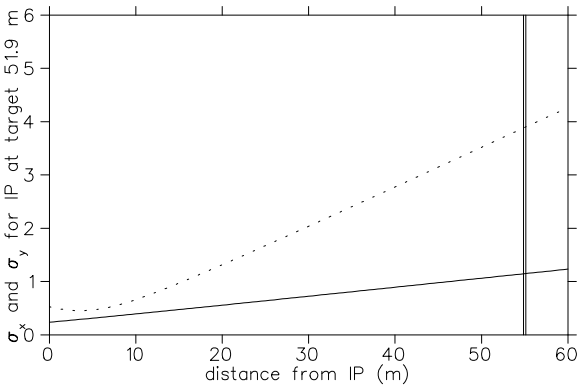

Figure 11. The horizontal (dotted line) and vertical (solid line) backscattered photon beam widths as a function of the distance from the IP. The IP is at 51.9 m from the target. The calorimeter position at 106 m from the target is indicated with the vertical double line.

As we now follow the backscattered photons towards the calorimeter, no interference with any beam element is found prior to the bending magnet 90 BH, which is the first bending magnet after the IP. Fig. 12 displays the region from 90 BH to 113 QL. It also shows the two sections **A** & **B**, which will be discussed below:

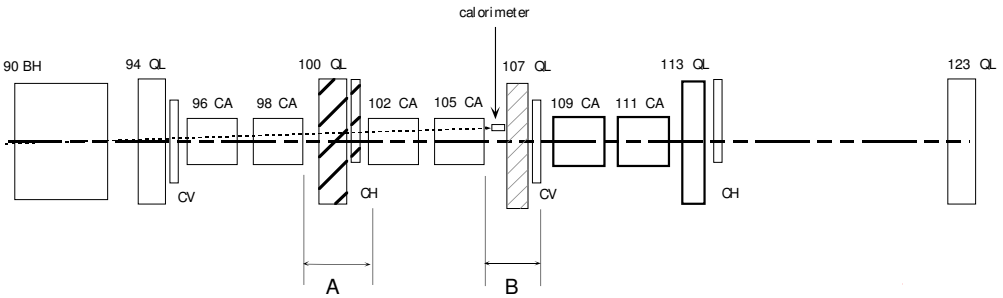

Figure 12. View from above of the cavity section between 90 BH and the 123 QL. The shaded areas (section **A** and **B**) require modifications to the storage ring.

It is required that there is no obstruction to the backscattered photons up to a width of at least ± 3 sigmas (to contain 99.7% of the distribution). If one also allows for orbit changes of about one sigma in x and y, no aperture should be smaller than ± 4 sigmas. Therefore, the photons would interfere with the beam pipe wall near the entrance of cavity 102 CA in section **A**; see Table 3. There, the backscattered photon beam is separated by 3.0 cm from the electron beam and has a width of 3.5 mm. This requires that the conventional beam pipe has to be modified. The horizontal aperture of the beam pipe must be increased from ± 4.0 cm to at least ± 4.4 cm.

The next modification to the beam pipe has to be at the exit of cavity 105 CA. There, the backscattered photon beam is separated by 4.1 cm from the electron beam and has a width of 3.8 mm. The diameter of the cavity opening is 12 cm. Since we require that there is no obstruction to the backscattered photons up to a width of ± 4 sigmas, the photons would interfere with the beam pipe walls in section **B**. Fortunately, the Beta-function is small (10 m) in that section. This does allow us to install a smaller, 40 mm round beam [17] with a 1.5 mm wall thickness. With this modification the NBW crystal can be installed right next to the beam pipe between 105 CA and 107 QL, and no cavities have to be removed.

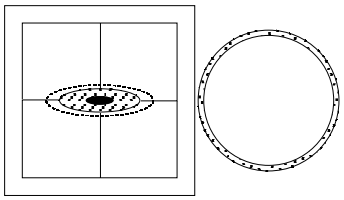

Figure 13. Cross section through Compton calorimeter and beam line. The gap between the beam pipe and the calorimeter is 0.1 mm. This close proximity to the beam line prohibits horizontal movements of the calorimeter. Therefore, the beam has to be tuned horizontally with special steering coils installed in the laser-electron IP. Also shown are the widths, σ_x and σ_y, (black area) of the Compton photons and their ± 3 sigma spread in the horizontal and vertical directions (shaded area) are shown. The dashed line includes the effect of ± 1 sigma orbit changes. The NBW crystals are shielded by a tungsten box with 4 mm thick walls. The round beam pipe is a non-standard piece and the electron beam does not go through its center.

H. Background

There are two important backgrounds which must be considered. One is the rather intense synchrotron radiation environment near 0°. The other background is from beam-gas bremsstrahlung, either coming from vacuum rest gas or the internal-target gas employed by the HERMES experiment.

1. Synchrotron Radiation Background

The polarimeter will be illuminated by the synchrotron radiation from the 90 BH bending magnet (2.7 mr). The number of photons radiated per second per mA machine current greater than ϵ_μ (keV) in a 1 m long bending magnet section is [19]:

$$N = 4.6 \times 10^{16} \frac{E^{2.5}}{\rho^{1.5}} \frac{1}{\sqrt{\epsilon_\mu}} \exp\left(-\frac{0.45 \epsilon_\mu \rho}{E^3}\right), \tag{14}$$

where E is the electron beam energy in GeV and ρ the bending radius of the magnet in meters.

For the 90 BH bending magnet ($\rho = 1244$ m), the rate of synchrotron photons per m per mA with energies above 1 MeV is 268 Hz, assuming a 27.5 GeV beam. For a current of 60 mA and a circulation frequency of 47 kHz, one photon per bunch with energy above 1 MeV will reach the detector. While the maximum energy of the synchrotron radiation is small, there is typically a very large energy flux. Thus the integrated energy deposited in the detector is 2×10^3 GeV per bunch, assuming a shielding of 3 mm lead to suppress the low energy photons. In order to get less than 100 MeV of energy deposited in the detector 17 mm lead shielding is required. That corresponds to 3.0 X_0, which has little effect on the NBW detector resolution. It deteriorates the resolution by a factor 1.1. We are studying the effect of this absorber on the energy weighted asymmetry. It is not assumed to make a large effect because cutting the low energy part of the energy weighted spectra (see Fig. 5) has very little effect on the asymmetry. And it can be simulated very accurately [20].

a) Vacuum Pressure:

The total cross section for emission of photons with energy greater than ϵE is given by [21]

$$\sigma(\epsilon) = 57.3\text{mb} \times [6.37\epsilon - 6.37\ln(\epsilon) - 2.34\epsilon^2 - 4.03], \tag{15}$$

where E is the electron beam energy in GeV. Assuming a beam line vacuum pressure of 6×10^{-9} Torr, the average nuclear charge of the gas atoms to be 5, and a beam current of 1 mA, the counting rate of photons with energy between 1 and 27.5 GeV is about 132 Hz per meter. Integrated over a beam length of 50 m and assuming 60 mA beam current this is about 397 kHz. If the energy cut is reduced to 100 MeV the rate is about 750 kHz. Since the bunch frequency is 10 MHz, the background rate per bunch is 0.08. The background rate should not be more than 0.01 to ensure that the probability of double scattering per bunch is not above 1%.

For the multi-photon method, the backscattered Compton rate is of order 1000, and therefore the background from vacuum rest gas can be totally neglected.

b) Target:

The bremsstrahlung background from the target is much more difficult to deal with. For a 10^{15} cm^{-2} target (Z=1), the rate is expected to be around 63 MHz for photon energies in the range of 100 MeV to 27.5 GeV. The best situation, where the calorimeter does not see any of the target bremsstrahlung, cannot be realized, unfortunately. It is therefore very important to shield the detector from these high rates. If we assume we take data 14 hours per day for a duration of 8 months with 60 mA beam current, 1.5×10^7 rad per year would be deposited in the NBW crystals.

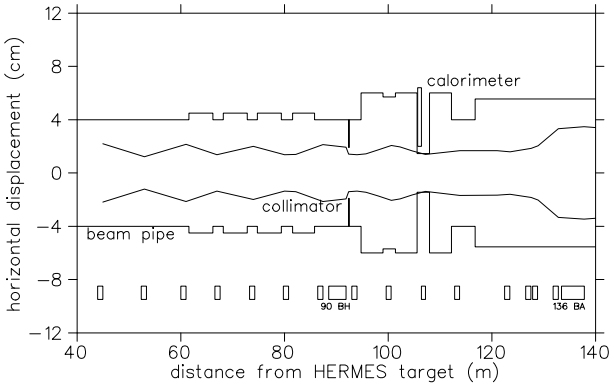

Figure 14. The proposed layout of the beam line between 40 m and 140 m from the target is shown. The calorimeter is at 106 m and the collimator at 92.4 m from the target. Also shown is the closest distance any aperture can be to the electron beam which is determined by the Beta-function and the relation: closest distance in mm = 40 mm $\sqrt{\beta(\text{m})/80\text{m}}$.

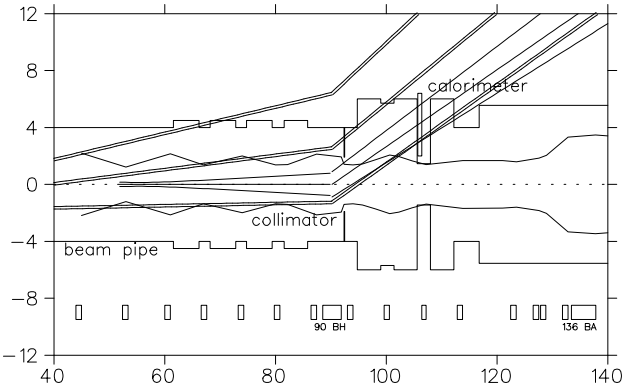

Figure 15. Same layout as Fig. 14. But overlaid are the $\pm 3\sigma$ distributions of the Compton photons (solid lines) and the bremsstrahlung photons (double lines). The necessity for the multi-photon technique and the collimator at 92.4 m from the target is very evident. Note, the kink in the photon distribution at bending magnet 90 BH is artificial.

The proposed layout of the longitudinal polarimeter has tried to take this into account. The laser-electron beam interaction region is about 52 m downstream of the target cell, after the first weak bending magnet (0.5 mr bending power). The calorimeter is about 16 m away from the second bending magnet (2.7 mr bending power). Fig. 14 shows a schematic layout of the longitudinal polarimeter. Fig. 15 also includes the ± 3 sigma distributions of the Compton and target bremsstrahlung photons. It can be clearly seen that the calorimeter would be sprayed with bremsstrahlung photons. We therefore propose to install a collimator between 90 BH and 94 QL at about 92.4 m from the target. Details are shown in Fig. 16. It needs to be

about 20 radiation lengths thick to absorb the bremsstrahlung photons (i.e. 7 cm of tungsten) and it should not limit the operation of the electron beam. As shown in Table 3, the horizontal Beta-function β_x is about 10 m, so a collimator with a $\pm$14 mm horizontal aperture and a $\pm$10 mm vertical aperture could be installed in the beam pipe without affecting the operation of the electron beam [17]. But the horizontal aperture has to be large enough not to cut into the backscattered photon distribution. Therefore, the collimator has to have $\pm$17 mm horizontal aperture. This is big enough to absorb a large fraction (94%) of the target bremsstrahlung photons (σ_x(92.4m) = 10.8 mm, σ_y(92.4m) = 4.4 mm). The beam optics parameters at the target used are α_x = 0.024, β_x = 2.47 m, and α_y = -0.013, β_y = 0.982 m.

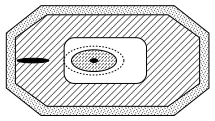

Figure 16. Cross section through the beam line at 92.4 m from the target. The electron beam, which is not shown, goes through the center of the beam line. The backscattered Compton photons are shown inside the collimator aperture which is $\pm$17 mm horizontally and $\pm$10 mm vertically. The collimator absorbs a large fraction of the target Bremsstrahlung photons whose horizontal and vertical half-widths are shown on the left side, near the beam pipe. The center of the bremsstrahlung distribution is 15.5 mm away from the collimator aperture. The backscattered Compton electrons are not shown here. Note that the collimator has to be cooled because it is hit by the synchrotron radiation produced by 90 BH.

The high background rates dictate the use of the multi-photon method in order to operate in parallel with HERMES data taking. The single photon method could have been used requiring however that:
a) the target gas flow be set to zero during a polarization measurement. (Note, it takes time to pump out all the gas from the thin transfer tubes). This would have led to a significant reduction in statistics for the HERMES experiment.
b) that the beam vacuum pressure be reduced by about a factor 10–20. This would have required many more new pumps in the electron-laser IP.

Table 3. A list of the magnet components and the horizontal Beta-functions at these locations is given. Also shown are the separations of the target bremsstrahlung photons and of the Compton photons from the electron beam. In addition, the same information is given for the possible locations of the collimator and the Compton calorimeter.

Component	position (m)	β_x (m)	Target bremsstrahlung photon separation (mm)	Compton photon separation (mm)	Compton photon σ_x (mm)
90 BH	88.5	20.1	26.6	0	2.4
collimator	92.4	10.0	34.5	5.8	2.8
94 QL	93.0	9.6	36.5	7.5	2.9
96 CA	96.6	14.2	48.0	17.1	3.1
98 CA	99.0	18.9	55.7	23.5	3.3
100 QL	99.6	20.2	57.6	25.0	3.4
102 CA	101.4	18.2	63.3	29.8	3.5
105 CA entrance	103.8	13.6	71.0	36.2	3.7
105 CA exit	105.6	10.1	76.8	41.0	3.8
calorimeter	105.7	10.0	77.1	41.3	3.8
107 QL	106.2	8.9	78.7	42.6	3.9
113 QL	112.8	13.9	99.8	60.1	4.3

III. BUDGET NOTES

Table 4 gives a detailed hardware cost estimate for implementing the longitudinal polarimeter in HERA East. Modifications to machine elements are not taken into account. It is assumed that DESY is going to cover the costs for the beam line modifications and the laser infrastructure, and that the remote-control mirrors, built by R. Kaiser for the transverse polarimeter, can be utilized.

Table 4. Budget estimate for implementing the longitudinal polarimeter as discussed in this proposal. All costs are in 1995 US dollars. 10% contingency has been added to the costs.
The University of Pennsylvania is providing $ 137,500 of the total amount. The National Science Foundation (NSF) has agreed to provide additional $ 153,500; $ 72,000 has already been received and $ 81,500 is expected in 1996. Additional funds are provided by the University of Freiburg of order DM 150,000.

Item		Cost (US $)
Pulsed YAG laser, Infinity (40 W)		120,000
Laser Warranty (3 years)		50,000
Laser table		10,000
Laser optics, transport system		52,000
Laser polarimeter		21,000
Compton calorimeter		25,000
NIM crates		10,000
Data acquisition, computer, electronics		60,000
Slow control hardware		15,000
	Subtotal	363,000
	contingency (10%)	36,000
TOTAL		399,000

IV. MANPOWER

The HERMES collaboration, with Jo van den Brand (University of Wisconsin-Madison, USA, and NIKHEF, Netherlands) as spokesman and Mike Vetterli (TRIUMF, Canada) as deputy spokesman, consists of 202 physicists from 29 institutions in 10 countries. The members of the longitudinal polarimeter group are formed by collaborators from the University of Pennsylvania, University of Freiburg, TRIUMF, and DESY. Some of them have considerable expertise on the transverse polarimeter.

We will have two graduate students [G] and two postdocs [P] stationed at DESY to work full time on the construction and commissioning of the longitudinal polarimeter. They are supported by two additional postdocs not stationed at DESY and also by a software engineer and a technician [S]. All the manpower mentioned above will be provided by the University of Pennsylvania and the University of Freiburg. In addition to the manpower mentioned above, several faculty members [F] and DESY staff members are involved in the project. The abbreviations used are: faculty [F], post-doc [P], graduate student [G], and university staff [S].

S. Barrow[P], T. Fortune[F], P. Kutt[S], W. Lorenzon[F], M. Spengos[P], S. Rudnitsky[G], and R. Zurmuhle[F]
University of Pennsylvania, Philadelphia, USA

K. Königsmann[F], M. Beckmann[G](June-15), 2. Graduate Student[G](Sept-1), H. Fischer[P](Aug-1), 2. Post-doc[P](Dec-95), Technician[S](June-15)
University of Freiburg, Freiburg, Germany

O. Häusser[F], new Post-doc[P] (Aug-1)
TRIUMF, Vancouver, Canada

P. Schuler, N. Meyners -MEA, Th. Limberg -MPY (Liaison Experiment–HERA, Safety), H.-D. Bremer -MKI (Polarimeter Engineer–HERA), D. Barber -MPY, W. Beckhusen -MEA (East-Hall Engineer), HERMES Technician
DESY, Hamburg, Germany

V. SCHEDULE

SLAC and SMC are planning to continue their measurements on the spin structure functions in 1995. They will improve on their statistical and systematic uncertainties (see Table 1). Therefore, it is very important to be able to get soon the smallest systematic errors possible. An important step in that direction is an additional, independent measurement of the beam polarization. HERMES will be taking data with ^{1}H and ^{2}D targets in 1996, where they are not limited by statistics anymore. For that high systematic accuracy is required. Therefore, we propose to get the longitudinal polarimeter installed during the shutdown in winter 1995/96.

VI. CONCLUSIONS

We have performed detailed studies to build a longitudinal polarimeter in the HERA East Section for the HERMES experiment. A technical solution is presented to implement the device in the present electron storage ring. We have discussed the main sources of systematic uncertainties and believe that a 2-3% measurement is feasible.

We propose to use a pulsed YAG (532 nm) laser. multi-photons ($10^3 - 10^4$) will be detected with an energy resolution of $10\%/\sqrt{E(\mathrm{GeV})}$. The electron-photon interaction region will be built very similar to the system used for the transverse polarimeter.

The two different techniques to measure the beam polarization have been compared. The main differences of the two types of polarimeters have been discussed: For a beam polarization of 0.70 the transverse polarimeter measures a spatial asymmetry $\leq 100\mu$m, whereas the longitudinal polarimeter measures a energy asymmetry ≤ 0.11 (energy peaks are separated by 1770 GeV for 1000 photons/bunch).

Most sources of systematic uncertainties are different for the two polarimeters and therefore allow us to perform truly independent measurements of the beam polarization.

The importance of reducing the systematic uncertainties in the beam polarization leads us to conclude that both the longitudinal and transverse polarimeter should be developed to their maximum capacities.

---

[1] HERMES Technical Design Report, DESY-PRC 93/06, MPIH-V20 1993.
[2] Analysis from 14 risetime curves measured in Oct/Nov 1994.
[3] Tom Junk (Stanford/SLD), private communications.
[4] A.A. Sokolov and I.M. Ternov, Sov. Phys. Doklady 8 (1964) 1203.
[5] D.P. Barber, private communications.
[6] V. Bargmann, L. Michel and V.L. Teledgi, Phys. Rev. Lett **2** (1959) 435.
[7] D.P. Barber et al., NIM **A338** (1994) 166.
[8] Y.S. Derbenev and A.M. Kondratenko, Sov. Phys. JETP 37, $N^0$6 (1973) 968.
[9] The Cern Minuit fitting routines were used to fit the exponential rise-time curves.
[10] D.P. Barber et al., NIM **A329** (1993) 79.
[11] R. Kaiser, diploma thesis, University of Münster, Germany, DESY F35D-92-02 (1992).
[12] Gordon Cates (Princeton), private communications.
[13] T. Peterson, MKI DESY, private communications.
[14] O. Häusser, report to HERA polarimeter group.
[15] Norbert Meyners, MEA DESY, has produced plans.
[16] Thomas Benisch, luminosity group HERMES experiment, private communications.
[17] R. Kose, private communications
[18] R. Brinkmann, private communications
[19] K.-U. Scholz, Diplom Thesis, DESY internal Report PET-78/03 (1978).
[20] GEANT Monte Carlo code from CERN, Version 3.21.
[21] R. Schmidt, Diplom Thesis, DESY Internal Report M-80/04 (1980); R. Schmidt, PhD Thesis, DESY Internal Report M-82-22 (1982); R. Rossmanith and R. Schmidt, DESY Report 84-105 (1984).